ASSESSMENT OF A NEW DESIGN FOR A REACTOR CAVITY COOLING SYSTEM IN A VERY HIGH TEMPERATURE GAS-COOLED REACTOR

GOON-CHERL PARK*[1], YUN-JE CHO[1] and HYOUNG KYU CHO[2]
[1]Department of Nuclear Engineering
Seoul National University
San 56-1, Shillim-dong, Kwanak-Gu, Seoul, 151-742, Korea
E-mail : senil0@snu.ac.kr
[2]Department of Thermal-Hydraulic Safety Research
Korea Atomc Energy Research Institute (KAERI)
150 Dukjin-Dong, Yuseong-gu, Daejeon, 305-353, Korea
E-mail : cho038@snu.ac.kr
*Corresponding author. E-mail : parkgc@snu.ac.kr

Received January 31, 2006

Presently, the VHTGR (Very High Temperature Gas-cooled Reactor) is considered the most attractive candidate for a GEN-IV reactor to produce hydrogen, which will be a key resource for future energy production. A new concept for a reactor cavity cooling system (RCCS), a critical safety feature in the VHTGR, is proposed in the present study. The proposed RCCS consists of passive water pool and active air cooling systems. These are employed to overcome the poor cooling capability of the air-cooled RCCS and the complex cavity structures of the water-cooled RCCS. In order to estimate the licensibility of the proposed design, its performance and integrity were tested experimentally with a reduced-scale mock-up facility, as well as with a separate-effect test facility (SET) for the 1/4 water pool of the RCCS-SNU to examine the heat transfer and pressure drop and code capability. This paper presents the test results for SET and validation of MARS-GCR, a system code for the safety analysis of a HTGR. In addition, CFX5.7, a computational fluid dynamics code, was also used for the code-to-code benchmark of MARS-GCR. From the present experimental and numerical studies, the efficacy of MARS-GCR in application to determining the optimal design of complicated systems such as a RCCS and evaluation of their feasibility has been validated.

KEYWORDS : VHTGR, RCCS, Water Pool, MARS-GCR, CFX5.7, RCCS-SNU

1. INTRODUCTION

Hydrogen production with a high temperature gas-cooled reactor (HTGR) is considered to be one of the most promising nuclear applications of the near future as energy productions shifts from the lead current oil economy to a hydrogen-based economy. Accordingly, many nuclear-developed countries have actively researched development of the VHTGR (Very High Temperature Gas-cooled Reactor) as a next generation reactor (GEN-IV) [1-3].

Since the VHTGR will be operated under high temperature above 900°C, effective measures are needed to passively remove the disposal heat from the reactor during normal operation and afterheat during a postulated accident such as a loss of forced convection (LOFC) accident. A RCCS (Reactor Cavity Cooling System) installed in the cavity between the reactor vessel and the containment is designed to take fulfill this role by preserving the reactor vessel under the maximum allowable temperature during normal operation and protecting the reactor containment structure in the event of failure of all active cooling systems. Thus, the performance and reliability of the RCCS are considered to be critical factors in determining the maximum design power level related to the afterheat removal [4]. Nevertheless, the capacity of the RCCS must not be over-designed, because excessive parasitic heat losses are undesirable during normal operation. Also, the heat load distribution during long-term LOFC accidents can vary considerably with the characteristics of the accident, thus further complicating the design of the RCCS. Due to difficulties in optimizing the capacity of the RCCS, experimental studies for validation and numerical studies using the validated codes are necessary to determine the adequacy of the design.

Table 1. Type and Characteristics of RCCS in the HTGRs

Reactor	RCCS Coolant / Type	Secondary Coolant /Type
HTTR	Water Forced Convection	Water Forced Convection
HTR-10	Water Natural Convection	Air Natural Convection
PBMR	Water Natural Convection	Air Natural Convection
GT-MHR	Air Natural Convection	No Secondary cooling
MHTGR	Air Natural Convection	No Secondary cooling

Existing types of RCCS proposed in developed and developing HTGRs are summarized in Table 1 [2-6]. As summarized in the table, the cooling methods in the RCCS include forced convection of water and natural circulation of water or natural circulation of air. It was reported that the active water cooling RCCS has an efficient cooling capability and is easy to design in comparison with other RCCS [4]. In order for it to provide the same level of reliability as the passive cooling scheme, however, it needs to be endowed with complex features, such as active cooling systems, a secondary side cooling system, and a water purification system. Moreover, in the cases of over-design or operation, excessive parasitic heat losses are undesirable with respect to maintaining power. The passive water cooling RCCS can reject the afterheat efficiently and with high reliability, but it has been reported that there is significant uncertainty and complexity associated with the two-phase natural circulation phenomena in the boiling mode [6]. Meanwhile, the air cooling scheme has fewer failure modes and is more passive than the other approaches, but its design is problematic, because the air flow around the reactor pressure vessel deviates due to the effects of the nozzle locations [4, 6]. Also, due to the poor cooling capability of the naturally circulating air, a very high chimney is necessary in order to provide sufficient air flow to remove the afterheat.

In this study, RCCS-SNU, a new design for a water-pool type RCCS for HTGRs, is proposed. This system is expected to have better cooling capability than the air cooled RCCS and benefits from a simpler cavity configuration than the water cooled type. In order to estimate the licensibility of the proposed design, its performance and integrity were tested experimentally with a reduced-scale integral mock-up, as well as with a separate-effect test facility (SET) for the 1/4 water pool of the RCCS-SNU to examine the heat transfer and pressure drop and code capability. The present paper only introduces the test results for SET and validation of MARS-GCR, a system code for the safety analysis of HTGR developed in the Korea Atomic Energy Research Institute. In addition, CFX5.7, a computational fluid dynamics code, was also used for the code-to-code benchmark of MARS-GCR.

2. THE CONCEPT OF THE WATER POOL TYPE RCCS

RCCS-SNU is a water pool type RCCS that has been developed to overcome the weak cooling ability of the air-cooled RCCS and the complex cavity structure of the water-cooled RCCS. This system, unlike the natural circulating water-cooled RCCS, uses a water pool as a heat sink for the parasitic heat emission during normal operation and the afterheat generated during accident conditions. A schematic diagram of the water pool type RCCS is presented in Fig. 1 and the heat transfer process in the proposed RCCS is illustrated in Fig. 2.

The system consists of three main parts: a side water pool located beside the reactor vessels, an upper water pool located above the reactor vessel, and five trains of air cooling systems submerged in the water pools (4 in the side water pool and 1 in the upper water pool). During normal operation, the heat loss from the reactor vessel is transferred into the water pools via the cavity. The heat is removed by the forced convection of air flowing through the cooling pipes, so that the heat is finally released to the atmosphere by the air. For the redundancy of the RCCS, five trains of blower systems are installed independently and sufficient cooling should be sustained, even in the event that one of the five blower systems fails.

In the case of a LOFC accident caused by unavailability of the main reactor core cooling system, all afterheat should be passively removed by the RCCS, assuming the accompanying failure of all blower systems. RCCS-SNU is designed to passively absorb the afterheat by boiling off the water in the pools and releasing the generated steam to the atmosphere. The capacity of the water pool should be sufficient to allow passive cooling of the afterheat to continue for three days.

RCCS-SNU is similar to common water cooling systems presently in operation, but is expected to be easier to design and analyze, because of the simple geometry of the cavity cooling surfaces. It uses ambient air to release the afterheat to the atmosphere, and thus no additional cooling systems are necessary. Also, it is expected to have less uncertainty

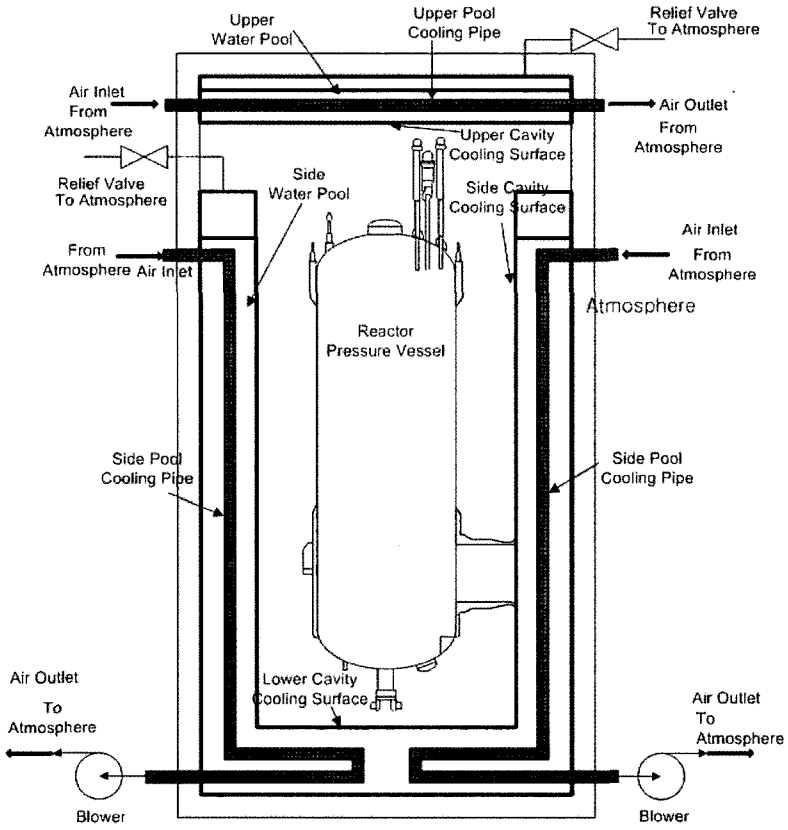

(a) System Configuration

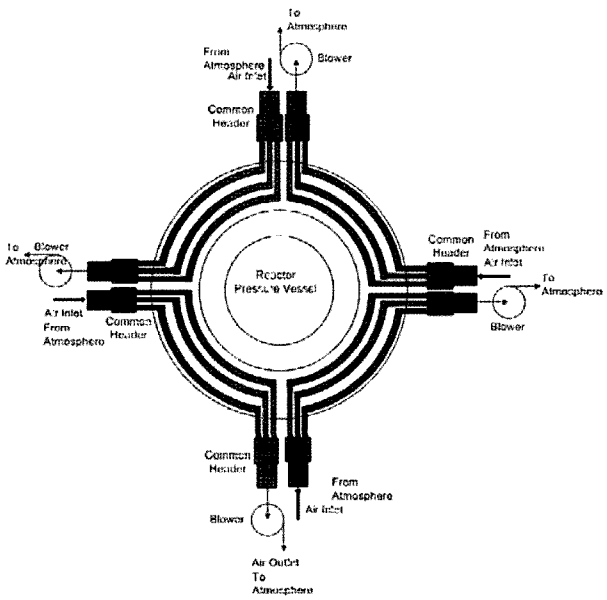

(b) Top View of the Side Water Pool

Fig. 1. System Configuration of RCCS-SNU

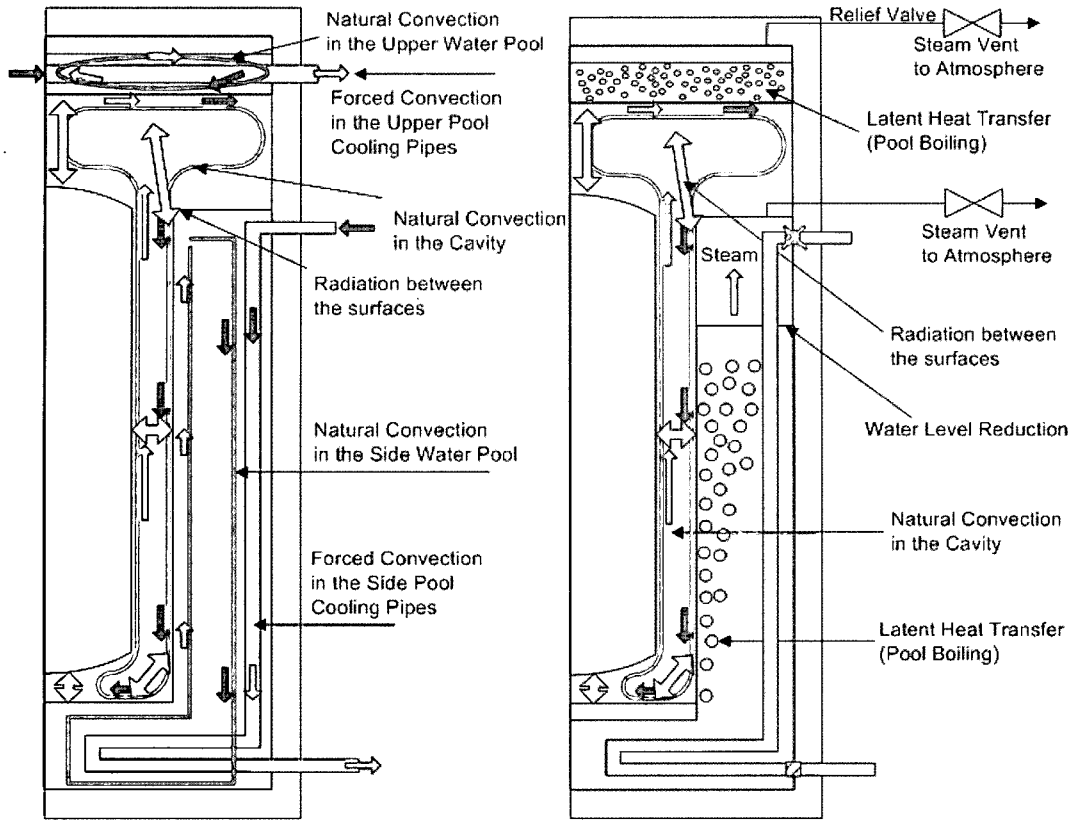

Fig. 2. Heat Transfer Process in RCCS-SNU

and complexity in the boiling situation than the other water cooling systems, since typical pool boiling occurs in the water pool of the system. The poor cooling capability of air, however, may require the air blower system to have an undesirably large capacity. Also, the size of the water pool needs to be optimized due to the limited space available inside the cavity.

For these reasons, we performed a series of experiments and numerical calculations to evaluate the feasibility of the water pool type RCCS and the cooling capability of the device.

3. RESEARCH APPROACH FOR VALIDATION OF NEW DESIGN

MARS-GCR, a thermal hydraulic system code, was selected to assess the performance of RCCS-SNU. MARS-GCR has been improved from the best estimate system code, MARS, which was developed by KAERI (Korea Atomic Energy Research Institute) for pressurized water-cooled reactor analysis [7, 8]. For the GCR analysis capability, fluid properties for He and CO_2 and heat transfer models, such as gas convection, radiation, and contact conduction, are incorporated into the code. Since the code has analysis capability of single and two phase forced convection, single and two phase natural convection, and radiation, it is expected to capable of predicting the thermal hydraulic phenomena in the water pool type RCCS if appropriate models such as heat transfer coefficient are incorporated. However, RCCS-SNU has complex geometry with three-fold helical cooling air pipes in the water pool. Thus, the applicability of a pseudo-multidimensional system for such complex flow geometry and different flow field combinations should be examined.

Thus, the applicability of the code for RCCS-SNU was assessed from experimental and numerical studies, as shown in Fig. 3. Two experimental test facilities are utilized, a reduced-scale mock-up test facility (IET) and a separate-effect test facility (SET) for the 1/4 water pool of the RCCS-

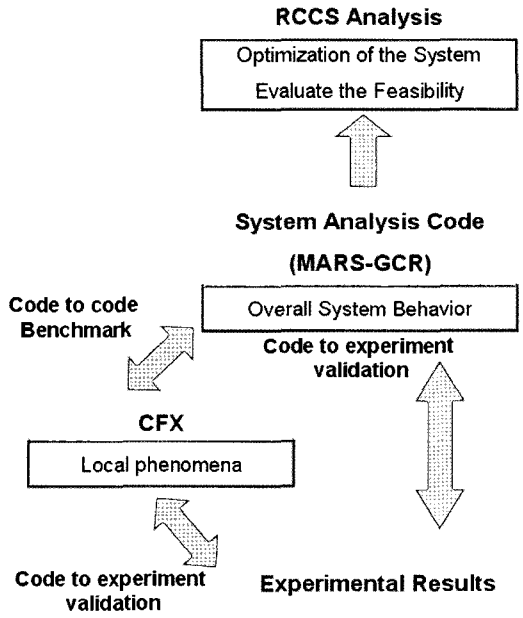

Fig. 3. Research Program for Validation of MARS-GCR

SNU. The former simulates all the heat transfer phenomena in the proposed RCCS including radiative heat transfer. Fig. 4 shows a schematic diagram of the test facility at 1/10 length scale and 1/100 power scale of a PBMR [9]. The geometry of the cooling pipes inside the water pools is presented in Fig. 5. Before simulating the IET test facility by MARS-GCR with full nodalization of the reactor vessel, cavity, water pools, and cooling pipes, it is necessary to confirm the adequacy of the constitutive relations in the code for the water pool of the proposed RCCS. To this end, a separate effect test was conducted by simulating a quarter section of the water pool of the IET test facility with a cooling pipe. The objective of the separate effect test is to assess the heat transfer correlations of the code, that is, the natural convective heat transfer model between the water in the water pool and the outer surface of the cooling pipe and the forced convective heat transfer model between the air flowing through the cooling pipe and its inner surface. The adequacy of the pressure drop calculation for such a zigzag-curved air pipe was also examined.

Although MARS-GCR is assessed in the scaled-down test facility, its applicability for the full scale water pool should be evaluated, because the correlations in the code

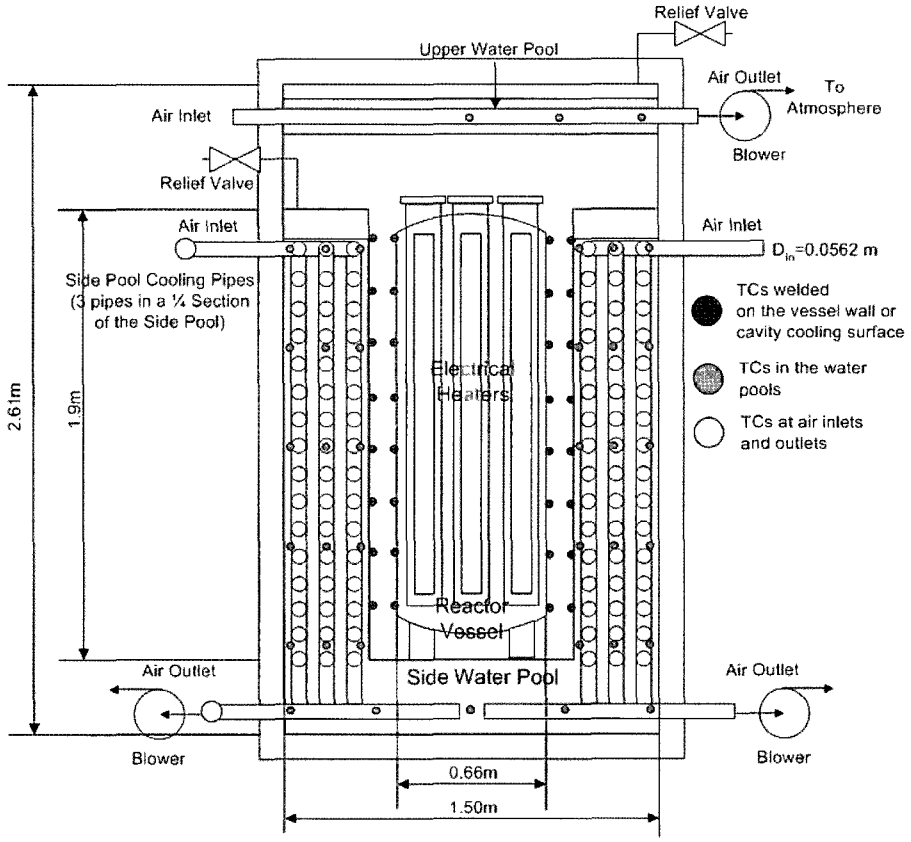

Fig. 4. Schematic Diagram of the RCCS-SNU IET Test Facility

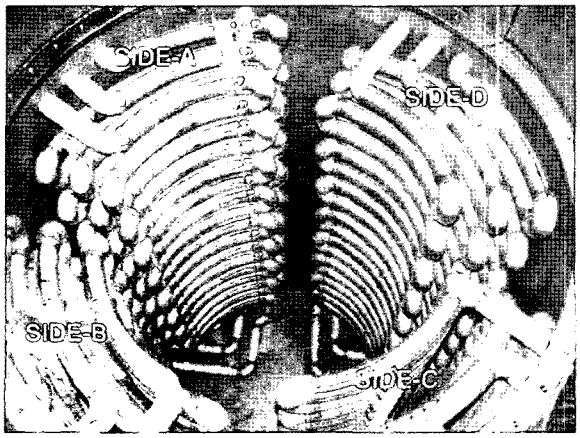

(a) Cooling Pipes in the Side Pool

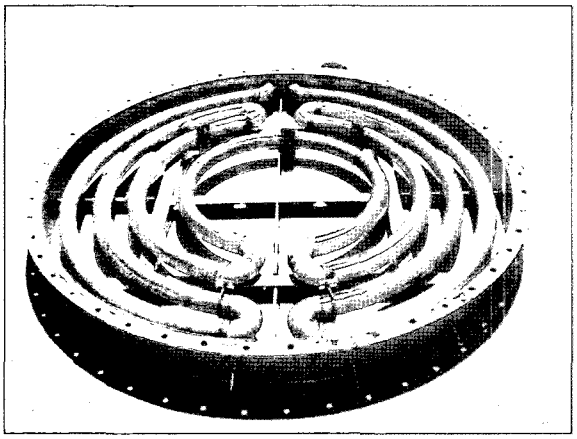

(b) Cooling Pipe in the Upper Pool

Fig. 5. Structure of Water Cooling Pipe

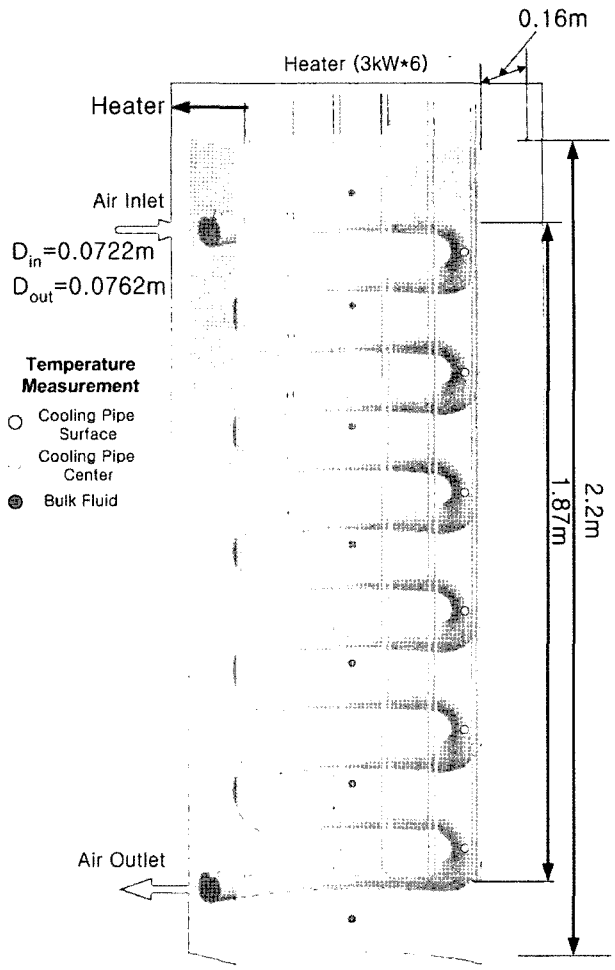

Fig. 6. Schematic Diagram of the Test Section for the Separate Effect Test

may be strongly dependent on scale effect. To address this problem, CFX5.7, a computational fluid dynamics code, is utilized for code-to-code benchmarking. CFX5.7 can also provide detailed information on the flow field in the water pool and is helpful to understand the heat transfer phenomena. For these reasons, a code-to-experiment benchmark for CFX5.7 was performed using the separate effect test results.

In this paper, only the separate effect test results are presented and the experimental results are compared with the prediction results of CFX5.7 and MARS-GCR as code-to-experiment benchmarks.

4. SEPARATE EFFECT TEST FOR RCCS-SNU

Figure 6 shows a schematic diagram of the test facility and the measuring parameters. The test section simulates a quarter section of the water pool and has six U-bend heaters in the vicinity of the inner wall to reproduce the heat from the cavity wall. To remove the heat, a cooling pipe is equipped in the test section. The cooling pipe has 11 times-fold U-bends, as shown in Fig. 6. The outlet of the cooling pipe is connected to the suction of a blower and ambient air flows through the cooling pipe. The major measuring parameters are the air flow rates, pressure drops along the cooling pipes, the water level in the water pool, and temperatures at the cooling pipe surface, cooling pipe center, and the water pool. The instrumentations, measuring locations, and their uncertainties are summarized in Table 2 and the location of the thermocouples is presented in Fig. 6.

The separate effect tests are steady state experiments and the test matrix is shown in Table 3. The steady state was confirmed through a comparison of the heating power and the heat removal rate. The heat removal rate by the

Table 2. Measuring Parameters and Instrumentations for the Separate Effect Test

MeasuringParameters	Measuring Location	Instrumen-tations	Uncertainty
Flow Rate	Cooling Pipe Inlet	Bi-directional Flow Tube	0.9 %
Temperature	Center : 12 Surface : 14 Liquid : 8	Thermo-couples	1.5 °C
Differential Pressure	Between Inlet and Outlet	DP Transmitter	0.6 %

Table 3. Test Matrix for Separate Effect Test

Power	Air velocity
3 kW	28, 33, 40, 48, 52 m/s
4 kW	28, 33, 40, 48, 52 m/s
5 kW	28, 33, 40, 48, 52 m/s
6 kW	33, 40, 48, 52 m/s

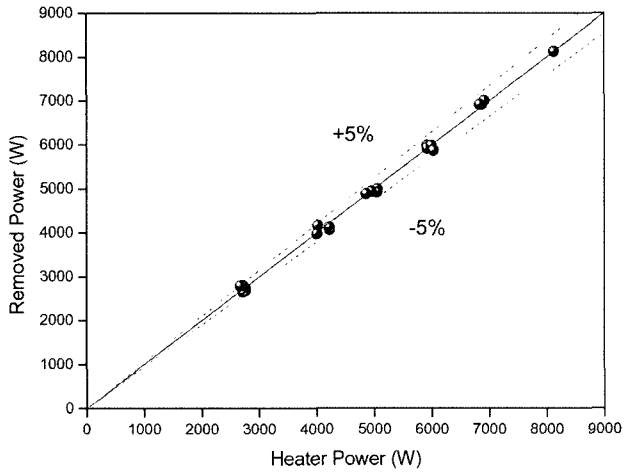

Fig. 7. Energy Balance of the Present Experiment

cooling pipe was calculated from the measurement of the flow rate and the temperatures of the inlet and outlet. Discrepancy of heat balances in the experiments was less than 5%, as shown in Fig. 7.

Fig. 8 shows the measure pressure drops and the pressure drop components between the inlet and outlet of the cooling pipe. The frictional pressure drop was calculated from Eqs. (1) and (2) applying the friction factor correlation of Nikuradse [10] for a smooth circular duct.

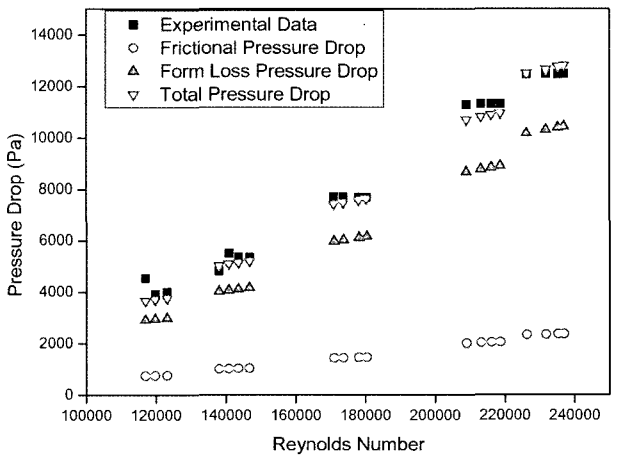

Fig. 8. Pressure Drop vs Re

$$\Delta P_{fric} = \frac{4fL}{D_h}\frac{\rho_g v_g^2}{2} \quad (1)$$

$$f = 0.0008 + 0.0553\,\mathrm{Re}^{-0.237} \quad (2)$$

The form loss pressure drop was calculated by the correlation of a standard U-bend [11] as,

$$K = \frac{K_1}{\mathrm{Re}} + K_\infty(1 + 0.5a^*) \quad (3)$$

where $K_1 = 1000$, $K_\infty = 0.35$ in U-bend.

Figure 9 shows reasonable agreement among the experimental data and the predicted total pressure drops. Thus, it was found that the loss coefficient of a standard U-bend can be applied to the cooling pipe of the water pool type RCCS. These experimental results for the pressure

drop and loss coefficient will be used as input values for the MARS-GCR calculation.

Figure 10 illustrates the experimental results of the axial temperature distributions in the water pool, and at the cooling pipe surface and the center of the cooling pipe for different inlet air flow rates. As air flows through the cooling pipe, the air temperature at the cooling pipe center increases gradually. However, the temperature of the cooling pipe surface shows little variation along the pipe axis and slightly decreases along the elevation, because relatively cold ambient air is drawn from the top part of the water pool. The bulk liquid temperature is higher at the top part of the pool than at the bottom part by only 1~2 °C. Thermal stratification is not significant in the water pool since a large portion of the heat is removed at the top part, where the water temperature varies significantly from the air temperature.

The average heat transfer coefficient inside the cooling pipe was calculated by using the measured temperatures as follows [12].

$$q_{conv} = \dot{m} c_p \left(T_{m,o} - T_{m,i}\right) = \bar{h} A_s \Delta T_{lm} \tag{4}$$

where, $\Delta T_{lm} = \dfrac{\left(T_s - T_{m,o}\right) - \left(T_s - T_{m,i}\right)}{\ln\left(\dfrac{T_s - T_{m,o}}{T_s - T_{m,i}}\right)}$,

T_s = Averaged-Surface Temperature.

$$\text{Therefore, } \bar{h} = \frac{\dot{m} c_p}{\pi D L} \frac{\left(T_{m,o} - T_{m,i}\right)}{\Delta T_{lm}} \tag{5}$$

The air inlet and outlet temperatures obtained from the experiments were used, and the surface temperature was obtained from the experiment values of the overall averaged temperature of the entire surface. These heat transfer coefficients in the experimental results were compared with well-known correlations for the heat transfer coefficient of a straight pipe, a helical coil, and a U-bend, as shown in Fig. 11. The Dittus-Boelter correlation [12] for a straight tube in a fully developed turbulent flow, the Mori-Nakayama correlation [13], the Tailby-Staddon correlation [14], and the Moshfeghian-Bell correlation [15] for a U-bend were used for the evaluation. These correlations are summarized in Table 4.

The experimental data are found to be about 20 % higher than the values predicted by Dittus-Boelter. It can be seen that the heat transfer coefficient in a curved pipe is always large than in a straight tube [16]. The Nusselt numbers from the experiments are about 20 % lower than those of the Mori-Nakayama correlation. The correlations

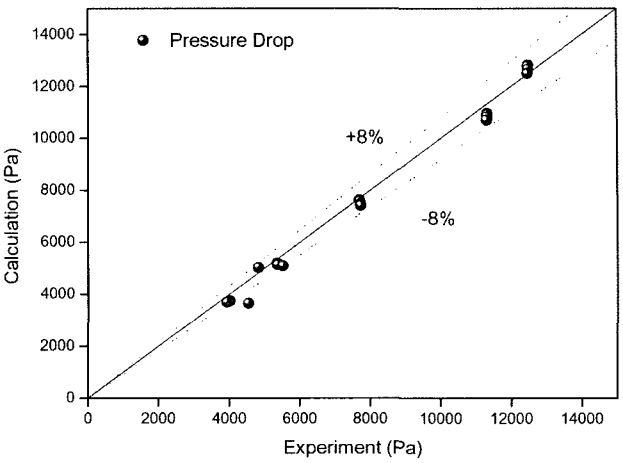

Fig. 9. Comparison of Measured Pressure Drop with Prediction

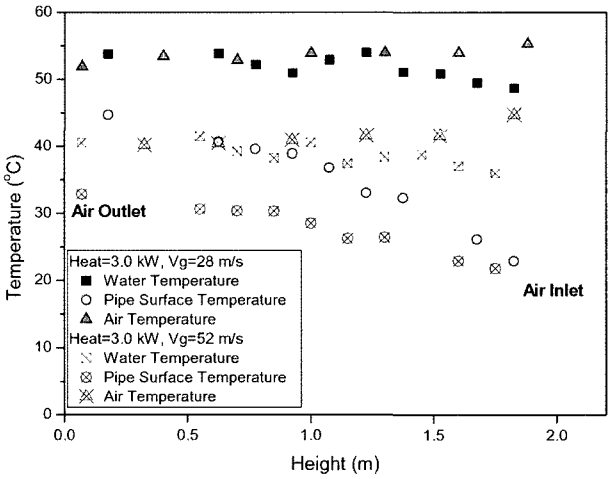

Fig. 10. Temperature Distribution in the Separate Effect Test

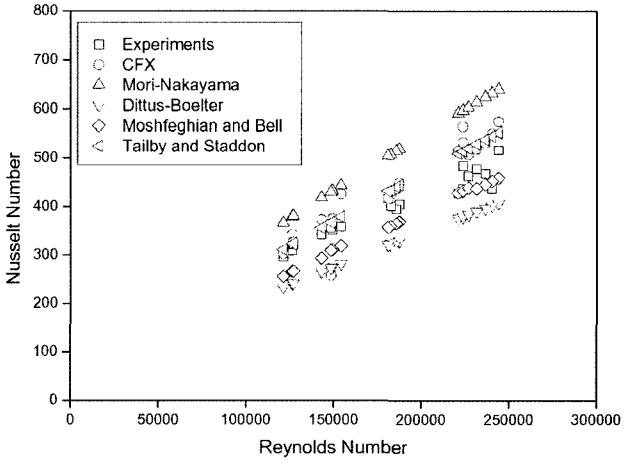

Fig. 11. Comparison of Heat Transfer Coefficients with Various Correlations

Table 4. Correlations of Heat Transfer Coefficient

	Correlation
Dittus and Boelter	$Nu = 0.023\mathrm{Re}^{4/5}\mathrm{Rr}^{0.4}$
Mori and Nakayama	$Nu = \frac{\mathrm{Pr}}{26.2(\mathrm{Pr}^{2/3}-0.074)}\mathrm{Re}^{4/5}\left(\frac{D}{D_{coil}}\right)^{1/10}\left[1+\frac{0.098}{\left\{\mathrm{Re}\left(D/D_{coil}\right)^2\right\}^{1/5}}\right]$
Moshfeghian and Bell	$Nu_x = 0.0931\left(\frac{D}{L}\right)^{-0.116}\mathrm{Re}^{0.825}\mathrm{Pr}^{0.4}\left(\frac{\mu_m}{\mu_w}\right)^{0.14}\left(\frac{R}{D}\right)^{0.884}\left[\left(1+\frac{L}{\pi R}\right)^{0.884}-1\right]$
Tailby and Staddon	$Nu_x = 0.0987\left(\frac{D}{L}\right)\mathrm{Re}^{0.82}\mathrm{Pr}^{0.4}\left(\frac{R}{L}\right)^{0.85}\left[\left(1+\frac{L}{\pi R}\right)^{0.96}-1\right]$

in the U-bend, which have been developed by Tailby and Staddon, Moshfeghian and Bell, are predicted in good agreement with the experimental data because the Tailby-Staddon correlation and the Moshfeghian-Bell correlation were developed based on the similar geometric structure.

These temperature profiles along the elevation and the calculated heat transfer coefficients were used for the code-to-experiment validation of CFX5.7 and MARS-GCR. In the following sections, the calculation results of those codes for the separate effect test are discussed.

5. ASSESSMENT OF MARS-GCR FOR SEPARATE EFFECT TEST OF RCCS-SNU

5.1 CFX5.7 Calculation Result

CFX5.7 calculations were done to investigate the characteristics of the heat transfer phenomena in the cooling pipe and to obtain detailed information of the fluid velocity and temperature. For simple calculation, the heat transfers in air inside the cooling pipe and water outside the cooling pipe were simulated independently.

First, the calculation results inside the cooling pipe are described. For the calculation, the experimental data of the cooling pipe surface temperature were adopted as wall boundary conditions. Fig. 12 shows the grid in the calculation and the standard k-e model was used for turbulence modeling. 177,540 nodes in total were used in a structured mesh. Figs. 13 and 14 show the calculated results for the velocity profile at various axial locations, and temperature profiles including the measured temperatures at the center of the cooling pipe. The centrifugal effect of the bend, which shifts the maximum of the axial velocity toward the outer

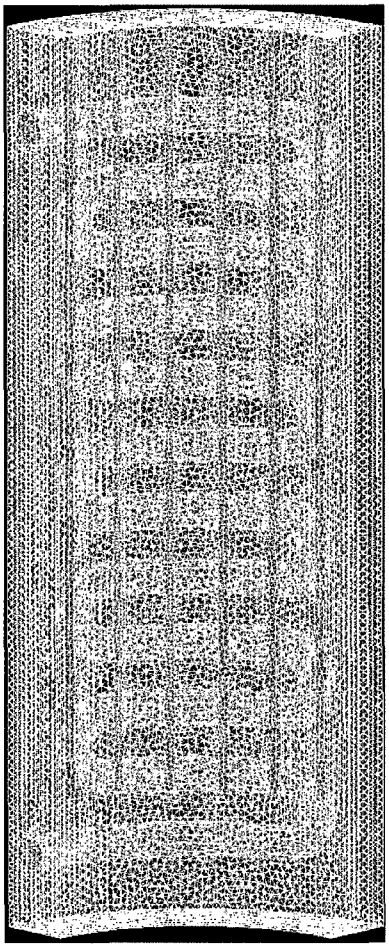

Fig. 12. Nodalization for the CFX5.7 Calculation

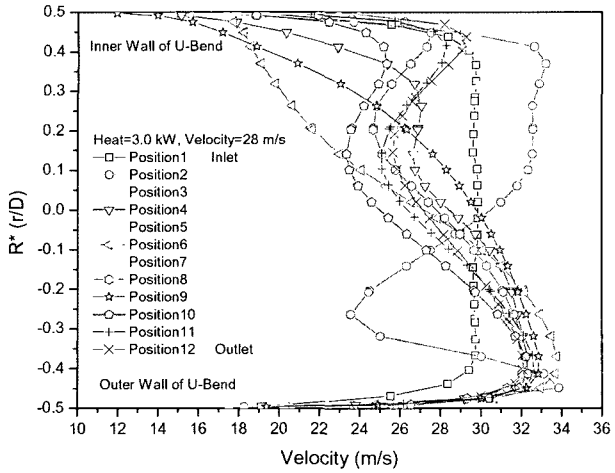

Fig. 13. Air Velocity Profiles in the Cooling Pipe

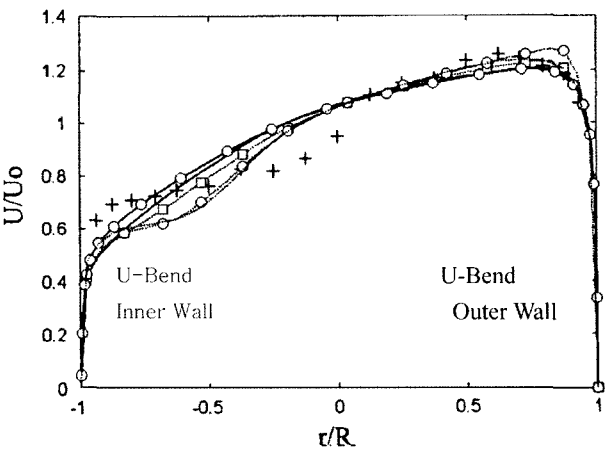

Fig. 16. Velocity Profile in the U-bend (Pruvost et al. [12])

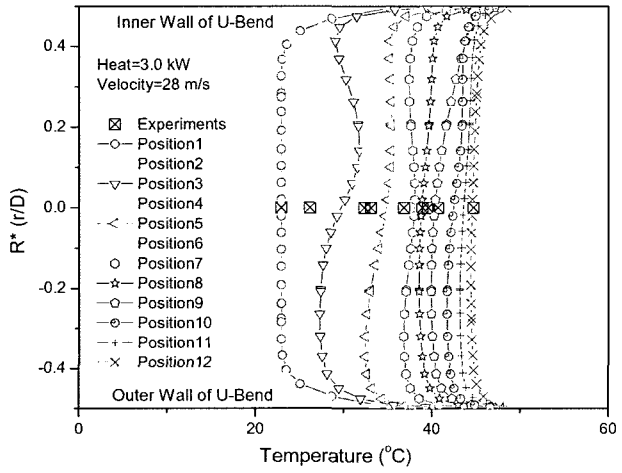

Fig. 14. Air Temperature Profiles in the Cooling Pipe

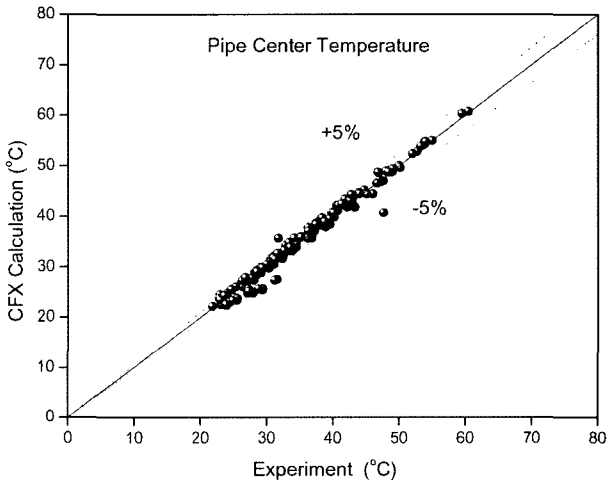

Fig. 17. Comparison of Pipe Center Temperature

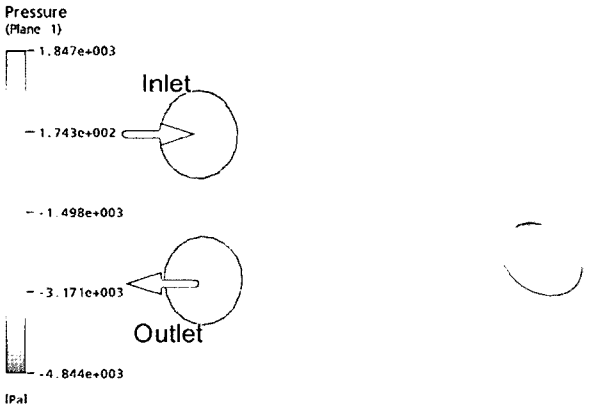

Fig. 15. Velocity at the Inlet and Outlet of the Cooling Pipe

wall, is represented well in our calculation, as shown in Fig. 15. This trend corresponds with the results of Pruvost et al. [17], who investigated the flow structure in a U-bend using the FLUENT code, as shown in Fig. 16. The present calculation results for the air temperature at the pipe center were also compared with the experimental results in Fig. 17. Although CFX5.7 slightly under-predicted the experimental data, the calculated temperatures showed reasonably good agreement with the experimental data.

Second, the calculation results for the water outside the cooling pipe are described. As for the above calculation, the experimental data of the cooling pipe surface temperature

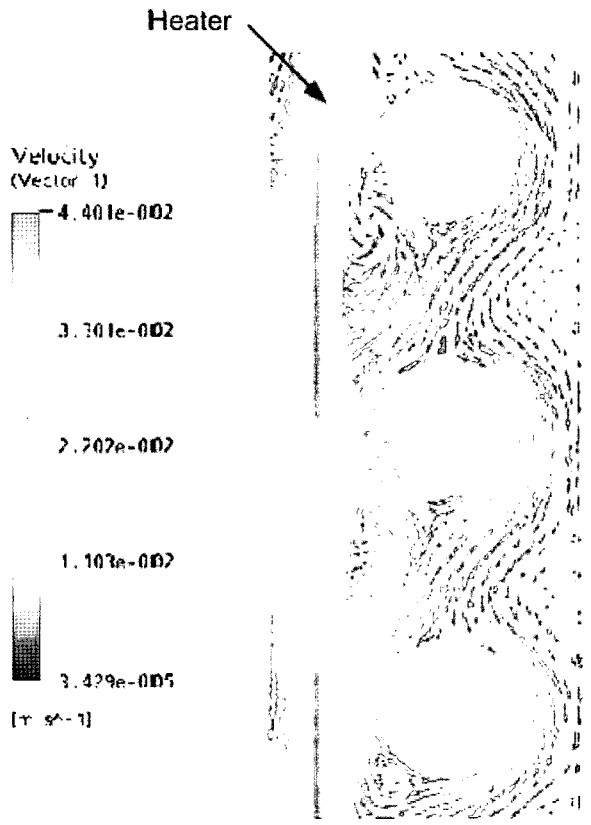

Fig. 18. Water Velocity Distribution in the Water Pool

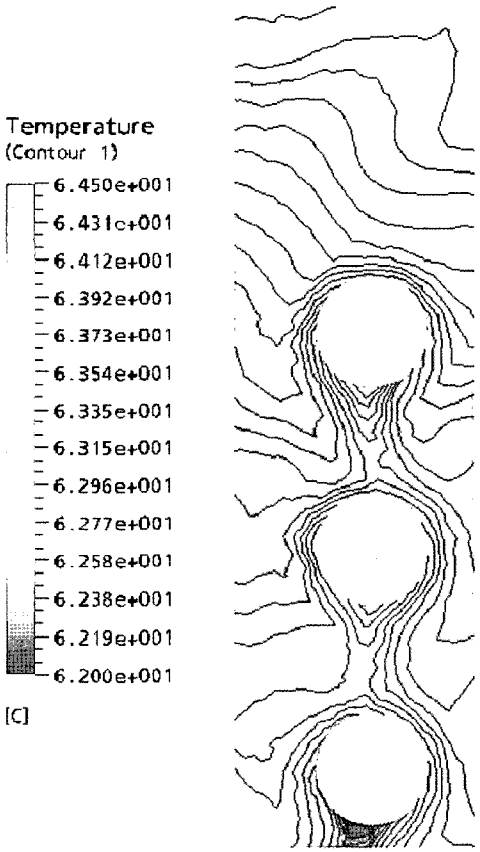

Fig. 19. Water Temperature Distribution in the Water Pool

were implemented as wall boundary conditions. 1,189,466 elements in an unstructured mesh were formed to model the water pool. Figs. 18 and 19 show typical calculation results for the velocity and temperature profiles in the water pool. Driven by buoyancy force, the heated fluid adjacent to the heaters begins to move upward at the bottom part of the heater and downward at the cooling pipe with a maximum velocity of about 1~2 cm/s. However, the velocity is much lower at the bottom region of the water pool, indicating that the fluid is stagnant there.

The calculated results for the water temperature in the pool are also compared with the experimental results in Fig. 20. As shown in the figure, the predicted water temperatures by CFX5.7 correspond well with those measured in the present experiment.

From these calculation results for the separate effect test facility, we concluded that CFX5.7 can simulate the heat transfer phenomena inside and outside the cooling pipe reasonably well.

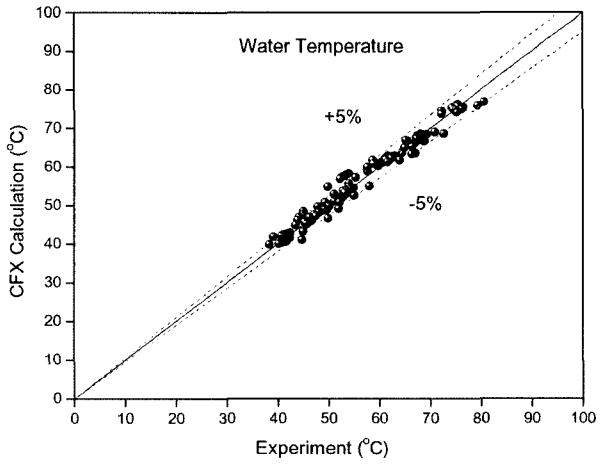

Fig. 20. Comparison of Water Temperature in the Water Pool

5.2 MARS-GCR Calculation Result

For the MARS-GCR calculation, the separate effect test facility was nodalized with 29 volumes, 33 junctions, and 31 heat structures, as shown in Fig. 21. The water pool was modeled using a multi-dimensional component, which consists of $2 \times 1 \times 7$ (r-θ-z) cylindrical coordinates. The cooling pipe was modeled as pipe component 211 with 12 volumes connected by 11 junctions. The water pool was radially divided by two nodes. Each node shares half of the air cooling pipe, which means each node has a preserved water volume with a heat structure of half the heat transfer area of the cooling pipe. The electrical power from six U-bend heaters was modeled as constant heat flux from 7 heat structures connected to the inner wall of the water pool. Air flows in the cooling pipe with constant mass through a time dependent junction 212 and a single junction 210 connected to the outlet and the inlet of the cooling pipe, respectively. Time dependent volumes 120, 200, and 220 were connected to trip valve 110, single junction 210, and time dependent junction 212, respectively, to simulate the ambient air.

The boundary condition for the MARS-GCR simulation corresponds to the test matrix, as shown in Table 3.

The cooling pipe surface of the water side and the heated wall in the water pool was represented by straight pipes when the water convection boundary condition was imposed. Inside the cooling pipe, the conditions of helical tube geometry were implemented for air convection. The MARS-GCR code uses the Churchill-Chu correlation for the heat transfer coefficient for natural water convection and the Dittus-Boelter correlation for air convection in the straight pipe [18]. The Mori-Nakayama correlation for air convection is used in the helical tube [13, 19]. Since the Mori-Nakayama correlation uses the ratio between the helical circle diameter and tube inner diameter, the radius of curvature of the cooling pipe was used as the helical circle diameter, as shown in Fig. 22.

MARS-GCR calculation results for the air temperature at the outlet of the cooling pipe were compared with the experimental data, as shown in Fig. 23, showing good

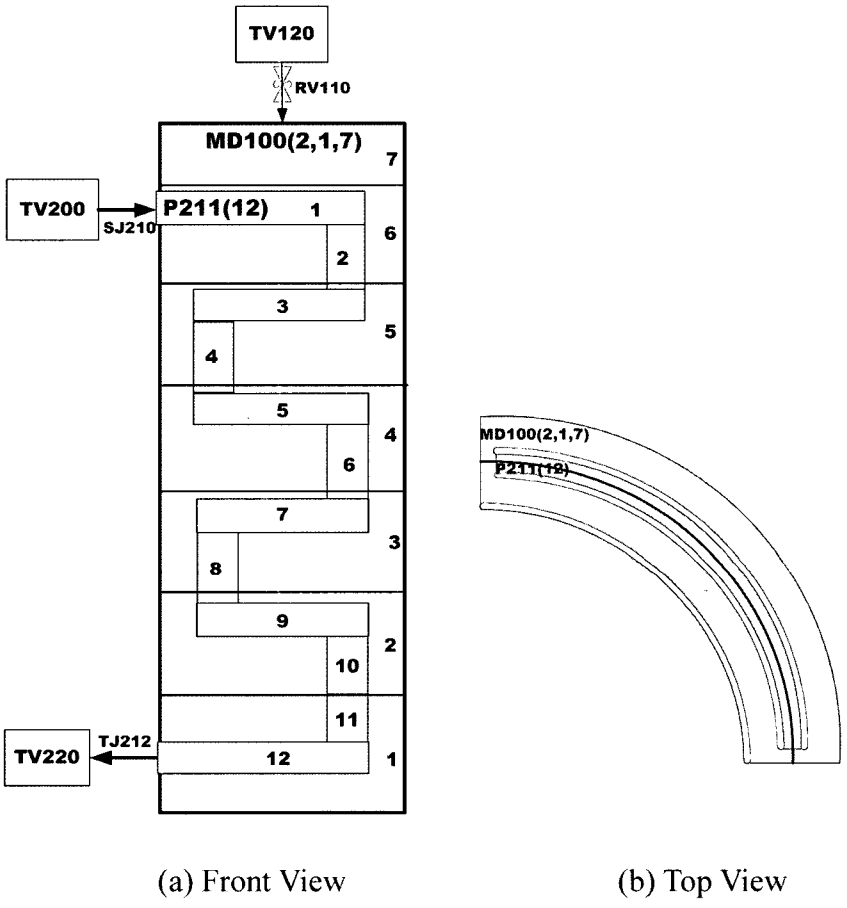

Fig. 21. Nodalization for the MARS-GCR Calculation

agreement.

Figure 24 shows calculation results for the axial temperature distributions of bulk temperature in the water pool, the pipe surface temperature, and the air temperature at the pipe center. Although the MARS-GCR code predicted the air temperature well, the pipe surface temperature and bulk water temperature were slightly under-predicted, as illustrated in Figs. 25 and 26. Under-predictions of the pipe surface temperature as well as the bulk temperature in the water pool are attributed to the inadequacy of the heat transfer coefficient correlation inside the cooling pipe, which was shown in the CFX5.7 calculation.

The fluid moves upward at the radially inner nodes near the heated wall and downward at the outer nodes with a maximum velocity of 1.5 cm/s in the water pool. This result shows good agreement with the CFX5.7 result and indicates that natural circulation is not significant in the water pool.

Figures 27 and 28 show the calculation results when inherent correlations in MARS-GCR for air convection were implemented inside the cooling pipe. Air temperatures at the pipe center show good agreement with the measured temperatures independently from the correlations because

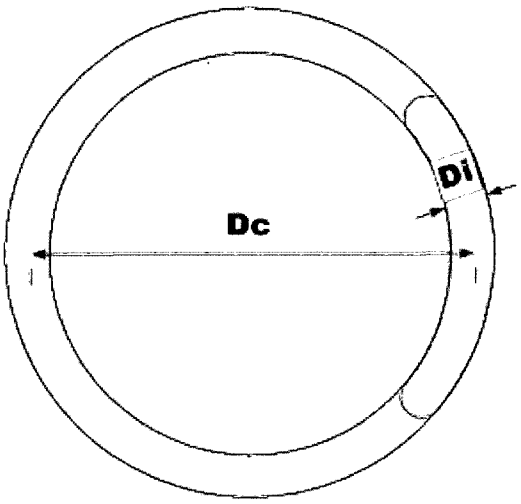

Fig. 22. Helical Circle Diameter-to-Tube Inner Diameter Ratio

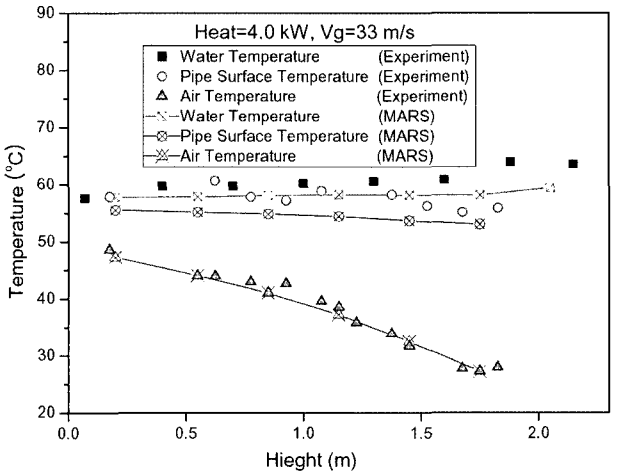

Fig. 24. Comparison of Temperature Distribution

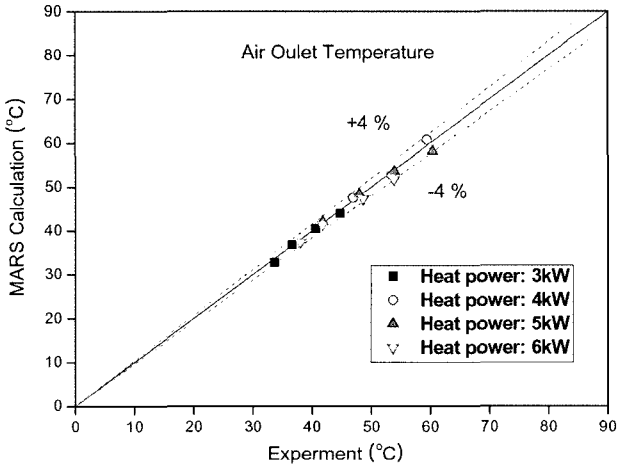

Fig. 23. Comparisons of Air Outlet Temperature

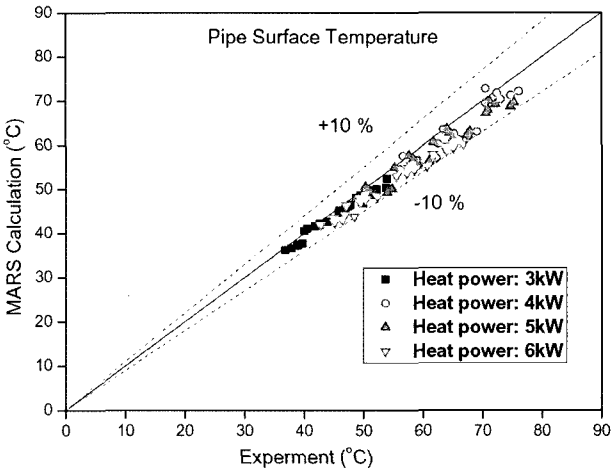

Fig. 25. Comparisons of Pipe Surface Temperature

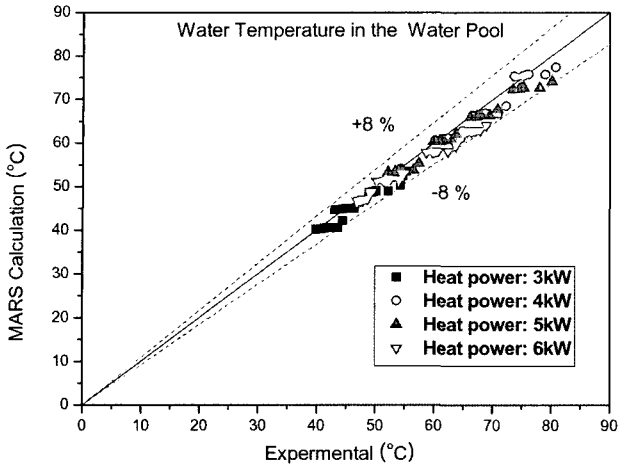

Fig. 26. Comparisons of Bulk Temperature in the Water Pool

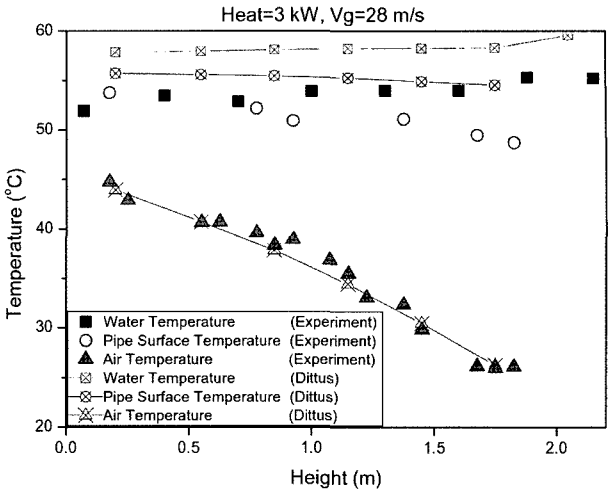

Fig. 28. Comparisons of Temperature Distribution with the Dittus-Boelter Correlation

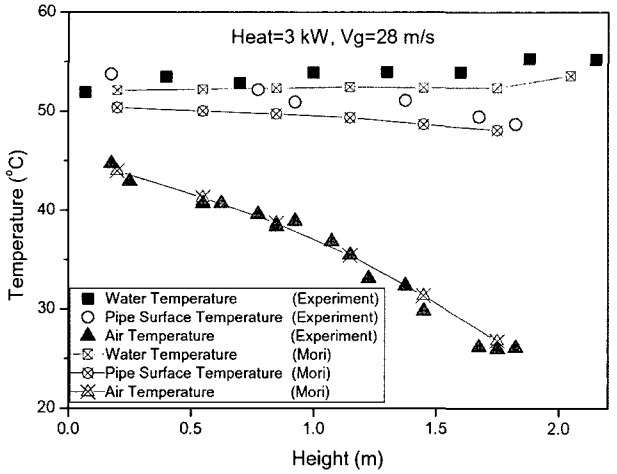

Fig. 27. Comparisons of Temperature Distribution with the Mori-Nakayama Correlation

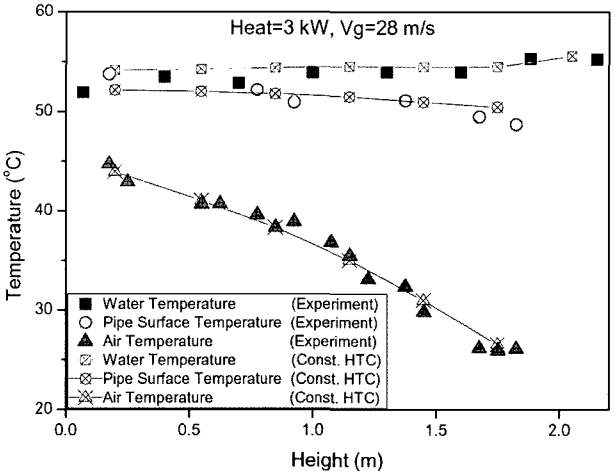

Fig. 29. . Comparisons of Temperature Distribution with Constant Heat Transfer Coefficient from SET

of the heat balance. However, the water and pipe surface temperatures were under-predicted when the Mori-Nakayama correlation was implemented, and over-predicted when the Dittus-Boelter correlation was implemented. These discrepancies are a result of the Mori-Nakayama correlation over-predicting the heat transfer coefficient and the Dittus-Boelter correlation under-predicting the heat transfer coefficient inside the cooling pipe, as verified in the CFX5.7 calculation.

In conclusion, MARS-GCR accurately predicts the heat transfer phenomena by natural convection inside the water pool. On the other hand, the heat transfer by forced convection of air inside the cooling pipe shows discrepancies with the experimental data when the Mori-Nakayama correlation and the Dittus-Boelter correlation are respectively implemented. However, the MARS-GCR calculation results

with the heat transfer coefficient from the experimental data inside pipe show good agreement with the experimental results for the temperature distribution of the pipe surface, the water in the water pool, and the air at the pipe center, as shown in Fig. 29.

6. CONCLUSIONS

This paper proposed a new water pool type RCCS design, named RCCS-SNU, which aims to overcome the poor cooling capability of the air-cooled RCCS and the complex cavity structures of the water-cooled RCCS. A separate effect test for the water pool of the RCCS-SNU was conducted to examine the performance of the new design and to provide experimental data for validation of MARS-GCR, which is being considered as an analytical tool for the proposed RCCS. The experimental data were also used for the code-to-code benchmark with CFX5.7. The CFX5.7 calculation results demonstrated that it can simulate the phenomena that occur inside and outside the cooling pipe reasonably well.

The MARS-GCR code predicts well the heat transfer phenomena by natural convection inside the water pool. On the other hand, the heat transfer by forced convection inside the cooling pipe shows discrepancies from the experimental data when the code-inherent correlations by Dittus-Boelter and Mori-Nakayama are respectively implemented. Thus, further investigations utilizing the MARS-GCR code are needed to precisely simulate the forced convection phenomena inside multiple U-bend pipes such as in the water pool type RCCS. Also, a future study with MARS-GCR for IET testing, which includes all heat transfer phenomena in the RCCS-SNU, is expected to demonstrate its analysis capability for radiative heat transfer and natural convective heat transfer in the cavity.

Nomenclature

A Area (m)
a^* Pipe radius (Inch)
C_p Specific heat (J/kg K)
D_h Hydraulic diameter (m)
De Dean number
f Friction factor
h Heat transfer coefficient(W/m^2 K)
K Loss coefficient
L Length (m)
Nu Nusselt number
ΔP Pressure drop (Pa)
Pr Prandtl number
Re Reynolds number
u Velocity (m/s)
$\dot{m}$ Mass flow rate (kg/s)

Greek Symbols

μ_m Viscosity of bulk mean temperature (Pa/s)
μ_w Viscosity of near wall temperature (Pa/s)
ρ_f Density of water (kg/m^3)

Subscripts

fric Friction
g Gas
i Inlet
o Outlet
lm Log mean
m Mean
s Surface
w Wall

REFERENCES

[1] M. Ogawa and T. Nishihara, "Present Status of Energy in Japan and HTTR Project," *Nuclear Engineering and Design*, Vol. 233, Issues 1-3, pp. 5-10 (2004).
[2] IAEA, "Heat Transport and Afterheat Removal for Gas Cooled Reactors under Accident Conditions," IAEA-TECDOC-1163, Vienna (2000).
[3] S. Saito et al., "Design and Safety Consideration in the High-Temperature Engineering Test Reactor (HTTR)," IAEA-TC-389, Dimitrovgrad (1989).
[4] Wu et al., "The Design Features of the HTR-10," *Nuclear Engineering and Design*, Vol. 218, pp. 25-32 (2002).
[5] IAEA, "Current Status and Future Development of Modular High Temperature Gas Cooled Reactor Technology," IAEA-TECDOC-1198 (2001).
[6] D.A. Dilling et al., "Passive Decay and Residual Heat Removal in the MHTGR," IAEA-TECDOC-757, Juelich (1982).
[7] W. J. Lee et al., "Development of MARS-GCR for Gas-Cooled Reactor Analysis – Incorporation of Gas Properties," *Proceeding of NURETH-10*, Seoul, Korea, October (2003).
[8] S. W. Lee et al., "Preliminary Sensitivity Study on Gas-Cooled Reactor for NHDD System Using MARS-GCR," *Proceeding of Korea Nuclear Society Autumn Meeting*, Busan, Korea, October (2005).
[9] PBMR Ltd., "Reactor Safety Analysis Report of the South-African Pebble-Bed Modular Reactor (PBMR)," *Rev. E, Centurion*, South-Africa (2000).
[10] S. Kakac, R.K. Shah and W. Aung, *Handbook of Single-phase Convective Heat Transfer*, A Wiley-Interscience publication (1987).
[11] W. B. Hooper, "The Two-K Method Predicts Head Losses in Pipe Fittings," *Chemical Engineering*, pp. 96-100 (1981).
[12] Frank P. Incropera, David P. DeWitt, *Introduction to Heat Transfer*, John Wiley & Sons, Third Edition (1996).
[13] Y. Mori and W. Nakayama, "Study on Forced Convective Heat Transfer in Curved Pipes," *International Journal of Heat and Mass Transfer*, Vol. 10, pp. 37-59 (1967).
[14] S. R. Tailby and P.W. Staddon, "The Influence of 90° and 180° Pipe Bends on Heat Transfer from an Internally Flowing Gas Stream," *Heat Transfer*, Vol.2 paper No. FC 4.5 (1970).
[15] M. Moshfeghian and K.J. Bell, "Local Heat Transfer Measurements in and Downstream from a U-bend," ASME paper No. 79-HT-82 (1979).
[16] G. W. Hogg, "The Effect of Secondary Flow on Point Heat Transfer Coefficients for Turbulent Flow inside Curved Tubes," Ph.D. Thesis, Univ. of Idaho (1968).

[17] J. Pruvost, J. Legrand and P. Legentilhomme, "Numerical Investigation of Bend and Torus Flows, Part I: Effect of Swirl Motion on Flow Structure in U-bend," *Chemical Engineering Science*, Vol. 59, pp. 3345 –3357 (2004).
[18] S. W. Churchill and H. H. S. Chu, "Correlating Equations for Laminar and Turbulent Free Convection from a Vertical Plate," I*nternational Journal of Heat and Mass Transfer*, Vol. 18, pp. 1323-1329 (1975).
[19] Zukauskas. A.A., *Heat Transfer from Tubes in Cross Flow*, Adv. Heat Transfer Academic, 8, pp.93-106 (1972).